Use of AXL-specific CAR T cells to treat non-small-cell lung cancer

Zhenfeng Zhang (✉ zhangzhf@gzhmu.edu.cn)
Second Affiliated Hospital of Guangzhou Medical University https://orcid.org/0000-0001-5621-9755

Bihui Cao
Department of Radiology, The Second Affiliated Hospital of Guangzhou Medical University
https://orcid.org/0000-0003-1161-7463

Manting Liu
Second Affiliated Hospital of Guangzhou Medical University

Yubo Zhou
Department of Library, Guangzhou Medical University

Qi Zhao
Cancer Centre, Faculty of Health Sciences, University of Macau

Lu Wang
Department of Radiology, The Second Affiliated Hospital of Guangzhou Medical University

Baoxia Liang
Second Affiliated Hospital of Guangzhou Medical University

Jinling Zhang
Second Affiliated Hospital of Guangzhou Medical University

Junping Li
Second Affiliated Hospital of Guangzhou Medical University

Xiaopei Chen
Second Affiliated Hospital of Guangzhou Medical University

Yunfei Feng
Second Affiliated Hospital of Guangzhou Medical University

Cheng Zhi
Second Affiliated Hospital of Guangzhou Medical University

Xin Yang
Department of Thoracic Surgery, The Second Affiliated Hospital of Guangzhou Medical University

Yu Tian
Department of Radiology, The Second Affiliated Hospital of Guangzhou Medical University

Yuling Hu
Second Affiliated Hospital of Guangzhou Medical University

Jinping He
Department of Radiology, The Second Affiliated Hospital of Guangzhou Medical University

Hong Hu
Department of Radiology, The Second Affiliated Hospital of Guangzhou Medical University
Xiaodie Ye
Second Affiliated Hospital of Guangzhou Medical University https://orcid.org/0000-0001-8447-1907
Guo Zhou
The Second Affiliated Hospital of Guangzhou Medical University
Aiming Chen
Qianjiang Central Hospital
Qingde Wu
Shunde Chinese Medicine Hospital, the Affiliated Hospital of Traditional Chinese Medicine University of Guangzhou
Linfeng Xu
Department of Interventional Therapy, Sun Yat-Sen Memorial Hospital, Sun Yat-Sen University
Ming Zhao
Sun Yat-sen University Cancer Center
Hui Lian
Second Affiliated Hospital of Guangzhou Medical University
Deji Chen
Second Affiliated Hospital of Guangzhou Medical University
Lili Yang
School of Public Health, Sun Yat-sen University

Article

Keywords: Chimeric antigen receptor, T cell, non-small cell lung cancer, EGFR, AXL, ablation therapy, tyrosine kinase inhibitor

Posted Date: February 16th, 2021

DOI: https://doi.org/10.21203/rs.3.rs-244810/v1

Abstract

The application of Chimeric antigen receptor (CAR) T cells in solid tumors is hindered by lack of tumor specific targets and inefficient T cell infiltration in tumor. It has been postulated that AXL may be an ideal immunotherapy target for non-small-cell lung cancer (NSCLC). Here, we screened 208 non-tumor samples from 22 types of human organs or tissues and 90 tumor samples from NSCLC patients by immunohistochemistry or Western Blotting and identified that AXL was rarely expressed in normal tissues but highly expressed in 69% NSCLC samples, suggesting AXL is an ideal target for CAR T cell therapy for lung cancer. We generated low-, mediate-, high-affinity AXL-CARs and evaluated their killing effect on NSCLC. Our data demonstrated antitumor effects of AXL-CAR T cell therapy for various NSCLC models both in vitro and in vivo. AXL-CAR T cells alone exerted strong antitumor effect in subcutaneous lung cancer cell derived xenograft (CDX), pulmonary metastases CDX, and intraperitoneal CDX models. Intraperitoneal delivery of CAR T cells resulted in superior tumor killing effects compared with systemic infusions for the intraperitoneal CDX tumor models. AXL-CAR T combined with microwave ablation (MWA) or EGFR-TKI resulted in enhanced killing effect and CAR-T cell infiltration in vivo. Together, our current study suggests that systemic or regional infusion of AXL-CAR T cell alone or combination with other therapies might have potential translatable value for the treatment of NSCLC in clinical situation.

Introduction

Despite great advances in current anti-cancer therapeutic strategies for local therapies including surgery, radiation, cold/thermal ablation and systemic therapies including chemotherapy, targeted therapy and immunotherapy, cancer prognosis remains poor due to distant metastasis[1]. Globally, lung cancer is the leading cause of cancer-related deaths, with non-small-cell lung cancer (NSCLC) as the most histological subtypes with a poor overall 5-year survival of ~15%[1,2]. Recently, epidermal growth factor receptor (EGFR) tyrosine kinase inhibitors (TKIs) have been widely applied in NSCLC patients. Unfortunately, this represents only part of lung cancer patients and drug resistance inevitably occurs[3]. Therefore, there is an urgent need for life-prolonging solution for the treatment of NSCLC patients[4].

Chimeric antigen receptor (CAR) T cell therapy has been proven as a potent approach for tumor treatment, especially the successful utilization of CD19-CAR T cells in B cell derived hematological malignancies[5,6]. Extending the clinical experience of CD19-CAR T cell therapy to solid tumors has been actively investigated[7]. However, the results of CAR T cell immunotherapy for solid tumors are not as notable as the outcomes for hematologic cancers[8]. Lack of specific antigen, inefficient infiltration of CAR T cells, immunosuppressive tumor microenvironment (TME), potential side-effects and antigen heterogeneity are currently considered as the main obstacles of CAR T therapy for solid tumors[9]. Besides optimizing structure and function of CAR T cells, novel delivery approaches of CAR T cells and varies of combination have also been explored. Previous preclinical data demonstrated that localized or intra-pleural transfer of CAR T cells showed potent antitumor efficacy in breast cancer and mesothelioma[10-12]. A case report indicated that intra-ventricular and intra-tumoral infusion of autologous CAR T cells

targeting IL13Rα2 mediated a transient complete response in a patient with recurrent multifocal glioblastoma[13]. Moreover, recent findings suggested that local photothermal therapy facilitated the accumulation and effective function of CAR T cells within solid tumors[14], suggesting that combinations among cellular immunotherapy with regional delivery and/or focal treatments could be particularly promising for solid tumor treatment and worth further exploration.

AXL is a typical oncogene and overexpressed in many human cancers[15,16], including lung, breast, colon, prostate, gastric, pancreatic, renal, esophageal, thyroid, liver, and ovarian cancers. Our previous study proved that the activation of AXL was required for epithelial-mesenchymal transition (EMT) and exhibited erlotinib resistance in EGFR-mutated NSCLC[17]. Since AXL is implicated in cancer progression and drug resistance, a therapeutic strategy targeting AXL could be a promising cancer therapy. As such, a series of AXL monoclonal antibodies, hMAb173 for renal cell carcinoma[15], D9 and E8 for pancreatic cancer[18], YW327.6S2 for NSCLC and breast cancer[19], have been shown robust anti-cancer efficacy in the preclinical and clinical trial stage. Moreover, AXL-targeted CAR T cells showed potent killing effect for various tumors. However, none of the researches above focused on non-small-cell lung cancer, and only monotherapies were involved in previous studies[20-22].

In current study, we constructed 3 types of AXL-targeting CARs with low-, mediate- and high-affinity to AXL and tested the therapeutic potential of these AXL-CAR T cell therapies for AXL positive NSCLC alone or in combination with local cell delivery, tumor ablation, and EGFR-TKI treatment by using multiple lung cancer cellular and animal models.

Results

Expression profile of AXL in human normal, NSCLC tissues and cell lines

AXL protein expression was evaluated and mild (1+) expression was observed in only two colon-rectum tissues among total 208 surgery samples from 22 types of non-tumor organs or tissues by IHC (Fig. 1a, Supplementary Table 1). AXL was detected by IHC in 62 out of 90 NSCLC (69%). In 30 out of 62 positive cases (48%), the AXL protein expression was moderate to strong, and was weak in 32 remaining cases (Fig. 1b, Supplementary Table 2). Notably, more cases with higher AXL expressed were found in EGFR-TKI resistance lung cancer tissues by IHC (Supplementary Table 2). Moreover, Western blotting (WB) analysis showed that average AXL expression level in EGFR-resistant NSCLC tissues was significantly higher than that in adjacent normal tissues (Fig. 1c). Among available lung cancer cell lines, AXL was detected high level in A549 and HCC827-ER3 (erlotinib-resistant cell line, as reported before), but not in HCC827 by WB and flow cytometry (Fig. 1d/e). These results demonstrated that AXL was expressed highly in NSCLC tissues, but rarely in normal tissues, indicating an ideal target of AXL as CAR T therapy for lung cancer. A549 and HCC827-ER3 cells were ideal cellular models for AXL-CAR T study with HCC827 as a negative control.

Generation of AXL-specific CAR T cells and in vitro antitumor cytotoxicity assay

We first verified the affinity of scFv from AXL monoclonal antibody to synthesized AXL protein by ELISA after expression and purification of scFv sequences[18,19,23,24] (Supplementary Fig. 1).

The CD3% of isolated primary human T lymphocytes reached 96.8%, 98.7%, and 99.2% in three healthy donors (Supplementary Fig. 2a). The AXL- or CD19-CAR molecules were comprised with anti-AXL or anti-CD19 scFv, a CD8 hinge, a CD28 transmembrane region, followed by the intracellular domains of co-stimulatory CD28, 41BB, and CD3ζ. T cells were transduced with AXL- or CD19-specific CAR vector to generate AXL- or CD19-CAR T cells (Fig. 2a). qPCR and WB results showed that CAR molecules were successfully introduced on the surface of AXL- and CD19-CAR T cells (Fig. 2b/c). The transduction efficiency of three AXL affinity 3E3E8-, YW327.6S2-, 20G7D9-, and CD19- CAR T were 25.3%, 29.1%, 30.5%, and 35.8%, respectively (Fig. 2d). Moreover, we observed similar phenotype changes of T cells before (on day 0, fresh T cells) and after transduction (on day 14, CAR T cells) (Supplementary Fig. 2b/c/d). These results indicated that the AXL-specific CAR T cells were transduced and expressed successfully; transduction with CAR molecules did not alter T cell phenotype.

To determine the cytotoxicity and cytokine secretion of AXL-CAR T cells against AXL-positive NSCLC cells in vitro, we performed a 24-hr killing assay of AXL- and CD19-CAR T cells on A549 GL (GFP and luciferase), HCC827 GL, and HCC827-ER3 GL cell lines. The in vitro results showed that AXL-CAR T cells exerted stronger cytotoxicity than CD19-CAR T or untransduced T cells after cocultured with A549 GL and HCC827-ER3 GL cells at the indicated effector T cell : tumor cell (E:T) ratios, especially at high E:T ratios. Whereas for AXL-negative HCC827 GL cells, cytotoxicity efficacy remained almost the same among AXL-CAR T, CD19-CAR T, and untransduced T cells (Fig. 2e/f). Among three AXL-CAR T cells, YW327.6S2-CAR T showed the strongest killing potency ($P<0.05$), which was selected for further studies. In the cytokine production assay, higher amounts of IL-2、TNF-α、IFN-γ、GM-CSF、Perforin and Granzyme B were produced by YW327.6S2-CAR T cells than CD19-CAR T or untransduced T cells in the presence of AXL-positive A549 and HCC827-ER3 cells compared to the presence of AXL-negative HCC827 cells (Fig. 3g). These results indicated that AXL-CAR T cells had an intrinsic target-dependent cytotoxic activity. Based on these findings, we proceeded to evaluate the therapeutic potential of YW327.6S2-CAR T cells in different in vivo lung cancer animal models.

YW327.6S2-CAR T cells induced tumor regression in subcutaneous lung cancer xenograft models

YW327.6S2- or CD19-CAR T cells were used to treat mice bearing established subcutaneous tumor xenografts formed by A549 and HCC827-ER3 cells (Fig. 3a/b, n=6). As shown in Fig. 3c-f, in the YW327.6S2-CAR T group, the calculated tumor volume remained almost unchanged, while tumor volume increased dramatically compared to the baseline (50 mm^3) in the Mock (PBS) and CD19-CAR T groups. Correspondingly, the measured average tumor weight in the YW327.6S2-CAR T group (A549 0.10g, HCC827-ER3 0.13g), was significantly lower ($P<0.001$) than that in the CD19-CAR T (A549 0.78g, HCC827-

ER3 0.60g) and Mock (A549 0.95g, HCC827-ER3 0.68g) groups (Fig. 3g/h). These results confirmed that YW327.6S2-CAR T cells had great potential for suppressing growth of AXL-positive lung cancer cells in the subcutaneous model by i.v. delivery.

YW327.6S2-CAR T cells showed killing potency in pulmonary metastatic models

To determine if YW327.6S2-CAR T cells can inhibit the distant metastasis of NSCLC, we developed an A549 GL bearing pulmonary metastatic models (Fig. 4a). Fourteen days after tumor inoculation via tail vein, tumor cells were detected in lungs (Fig. 4b), mimicking the pulmonary metastasis of NSCLC. We infused 1×10^7 YW327.6S2- or CD19-CAR T cells into these pulmonary tumor-bearing mice (i.v.) on the same day. Bioluminescence imaging (BLI) results demonstrated that YW327.6S2-CAR T cells almost eliminated pulmonary tumor cells in most mice on day 38, while CD19-CAR T or untransduced T cells could not control tumor cell progression (Fig. 4b/c). Significantly, pulmonary-colonized tumor cells caused mouse death within 62 days in the Mock and CD19-CAR T groups. In contrast, mice in the YW327.6S2-CAR T group continued to survive until day 90 (Fig. 4d). Finally, higher percentage of T cells was detected in peripheral blood of the YW327.6S2-CAR T group in 14 days after T cell infusion, indicating the expansion of CAR T cells in vivo (Fig. 4e). Collectively, our data demonstrated that YW327.6S2-CAR T cells exerted strong antitumor activity against AXL-positive NSCLC pulmonary metastatic tumor models in vivo.

Regional delivery of CAR T cells was more potent than the systemic approach

Intraperitoneal (i.p.) lung cancer metastatic mouse model was established with i.p. injection of A549 GL cells on day 0. On day 14, the mice were subjected to BLI, and robust intraperitoneal expansion of tumor cells was observed (Fig. 5a/b). These mice were then divided into three groups: Mock (PBS), YW327.6S2-CAR T (i.v.), and YW327.6S2-CAR T (i.p.). On the same day, mice were administrated with PBS or 1×10^7 effector cells (i.v. or i.p.). Surprisingly, YW327.6S2-CAR T cells, either i.v. or i.p., induced significant tumor regression of A549 GL bearing mice, while tumors in Mock groups continued to progress, as detected by BLI on day 21 and 35 (Fig. 5b/c). Obviously, bioluminescence signals in the abdominal cavity in mice with i.p. delivery showed strongest decrease on day 21 and day 35 compared to those in other two groups ($p < 0.05$) (Fig. 5c). The survival time of mice in the i.p. group was significantly longer than that in the Mock and i.v. groups ($p < 0.05$) (Fig. 5d). In addition, the persistence of CAR T cells was detected in the peripheral blood in 14 days after T cell infusion, and CAR T cell percentage in i.p. group was higher than that in i.v. group ($p < 0.05$) (Fig. 5e). Taken together, these results supported that i.p. delivery of CAR T cells resulted in superior tumor killing effect compared with systemic infusions for the intraperitoneal lung cancer models.

Microwave ablation promoted antitumor activity of CAR T cells and their infiltration in P.B. or tumor

To evaluate the therapeutic effect of YW327.6S2-CAR T combined with microwave ablation (MWA), subcutaneous tumor model by injecting HCC827-ER3 cells was firstly constructed on day 0. The following related study was initiated when tumor volume reached 200 mm^3. According to our power-time gradient research, we selected 10w and 45s as ablation parameters to achieve partial ablation, which faithfully mimicked the tumor residue after MWA therapy in clinical situation (Supplementary Fig. 3). The inoculated NSG mice were then allocated to (n=5): Mock (PBS), MWA (10w, 45s), YW327.6S2-CAR T (10^7 cells, intratumoral (i.t.)), MWA (10w, 45s) combined with YW327.6S2-CAR T (5×10^6 cells, i.t.) (Fig.6a). On day 54, the mean tumor weight was 0.02g in combination group where tumors were significantly smaller than those in YW327.6S2-CAR T (0.34g, $p < 0.01$), MWA (0.76g, $p < 0.001$) alone or Mock group (1.73g, $p < 0.001$) (Fig.6 b/c/d), with two tumors completely eradicated. Though only half of CAR T cell dosage was administrated in combination group, the percentage of infiltrated CAR T cells in P.B. or tumor was significantly higher in combination group than that in YW327.6S2-CAR T group (Fig.6 e/f). In addition, YW327.6S2-CAR T cells prevented the distant metastasis, while Mock or MWA group showed obvious metastasis lesion in the lung (Fig.6 g). Correspondingly, the weight of harvested lung was significantly lower in YW327.6S2-CAR T (0.21g) or combination (0.20g) group than that in Mock (0.34g) or MWA (0.26g) group (Fig.6 h). IHC results verified the metastatic tumor originated from the human HCC827-ER3 cells (HLA positive) (Fig.6i). No obvious damage could be observed in the organs from the mice treated with MWA or/and YW327.6S2-CAR T cells, which indicates a good safety threshold (Fig. 6j). Collectively, MWA combined with YW327.6S2-CAR T cells resulted in increased infiltration and accumulation of CAR T cells and exhibited superior efficacy against lung cancer, compared with each treatment alone. Also, administration of YW327.6S2-CAR T cells was safe to NSG mice.

YW327.6S2-CAR T cells combined with erlotinib induced decreased AXL intensity in EGFR-TKI resistant tumor, which restored the tumor sensitivity to erlotinib

We next investigated the antitumor activity of YW327.6S2-CAR T cells, erlotinib, or YW327.6S2-CAR T cells plus erlotinib in NSG mice with subcutaneous xenograft models established with HCC827-ER3 GL cells which are erlotinib-resistant due to AXL induction as reported before[17]. The treatment of the mice was shown in Fig. 7a and described in Materials and Methods. As shown in Fig. 7b/c/d, the combination of YW327.6S2-CAR T cells and erlotinib significantly reduced the growth rate of HCC827-ER3 GL tumors compared to erlotinib or YW327.6S2-CAR T cells alone. The tumors in NSG mice that received YW327.6S2-CAR T cells plus erlotinib treatment were almost eradicated. YW327.6S2-CAR T cells alone or in combination therapy induced decreases in AXL intensity within tumors at day 42, which was consistent with selection for tumor cell variants expressing lower levels of AXL (Fig. 7e). YW327.6S2-CAR T cells induced the most significant decrease in AXL expression when combined with erlotinib, and the decrease of AXL correlated with antitumor efficacy (Fig. 7f). These results further demonstrated that the YW327.6S2-CAR T cells and erlotinib had synergistic antitumor effects against AXL-positive NSCLC; AXL-

CAR T cells induced decreased AXL intensity, which restored the tumor sensitivity to erlotinib of EGFR-resistant NSCLC, consistent with prior report[17].

Discussion

Clinical application of CAR T cells faces a unique set of challenges against solid tumors. The major challenge for CAR T cell immunotherapy in NSCLC is to select a specific antigen that can discriminate tumor from normal tissue[8]. Homing of CAR T cells to the tumor sites must be sufficient and effective. Once infiltrating into the tumor, the CAR T cells have to survive, proliferate, persist, and mediate cytotoxicity in an unfriendly milieu largely composed of immunosuppressive mediators[25]. Moreover, infiltrated CAR T cells should be capable of recognizing the uniquely and homogeneously expressed tumor antigens displayed on a large degree of solid tumor cells. To induce a favorable antitumor outcome, CAR T cells have to fulfill the aforementioned arduous tasks.

In the present study, we have revealed that AXL might be an ideal target for NSCLC therapy. AXL expression was detected in 69% (62/90) of NSCLC cases, including 40 EGFR-TKI resistant tumors and rarely found in 22 kinds of human non-tumor tissues (Fig. 1a/b, Supplementary Table 1/2). AXL tended to be expressed higher in EGFR-TKI resistance NSCLC tissues than that in their adjacent normal tissues and non-EGFR-TKI resistance NSCLC (Fig. 1c, Supplementary Table 2). These results were consistent with previous studies[17,26]. High expression in lung cancer tissues and restricted expression in normal tissues made AXL an attractive target for CAR T immunotherapy. Furthermore, we verified that, when coculture AXL-positive NSCLC cells with AXL-targeted CAR T cells, an intrinsic target-dependent cytotoxic and cytokine secrete activity was largely stimulated in vitro (Fig. 2). AXL-targeted CAR T antitumor potency was observed both in subcutaneous or lung metastatic mice models in vivo (Fig. 3). More importantly, CAR T cells using scFv originated from YW327.6S2 (highest affinity to the AXL molecule in present study) as the antigen-binding element had no toxicities on mice normal tissues although the antibody could bind strongly to the mouse AXL protein (Fig. 6), suggesting that AXL could be a valuable and safe target for lung cancer immunotherapy.

Preclinical studies and case report delineated that regional administered CAR T cells including intra-ventricular, intra-pleurally, or intra-tumoral, vastly out-performed systemically infused T cells and induced potent antitumor efficiency[10-13]. In order to optimize cell delivery approaches, we compared killing effects of intraperitoneal with intravenous infusion of CAR T cells for treatment of intraperitoneal metastatic lung cancer models and demonstrated that i.p. delivery of CAR T cells induced superior tumor killing efficacy and the survival time, as well as CAR T cells infiltration in peripheral blood in the i.p. group were significantly longer and higher than those in i.v. group. This may attribute to early and direct antigen exposure and interaction facilitating activation and killing function of CAR T cells[12].

Thermal ablation has been proved to be an important technique in the treatment of inoperable lung cancer with frequently remained tumor residue and marginal recurrence[27,28]. In this study, we reported a novel regimen via combining YW327.6S2-CAR T cells and MWA, to treat lung cancer in mouse tumor

model. Excitingly, YW327.6S2-CAR T combined with microwave ablation yielded synergistic effect, which enhanced killing capability and prevented distant metastasis. Furthermore, the combination treatment increased CAR T cells infiltration both in tumor and peripheral blood (Fig. 6). The underlying synergistic mechanism is likely multifactorial: 1. tumor burden can be rapidly debulked (cell death occurring within minutes to hours) directly after MWA; 2. partial ablation can also reduce the density of solid tumor, interstitial fluid pressure, and loss of cell-cell adhesion in favor of mitigating the immunosuppressive microenvironment; 3. pro-inflammatory cytokines that are released from the ablated tissue or tumor cells, as well as the disruption of local extracellular matrix and tissue components provide a local inflammatory response, which may generate specific immunity, burst the CAR T cells activity and potentially control metastatic lesions [29]. All these factors may directly or indirectly result in increased infiltration, accumulation, and activation of CAR T cells[14,30]. Previous patient and animal studies also observed the similar phenomenon including inflammatory lymphocytes infiltrates (including T cells) and pro-inflammatory cytokines release after thermal ablation, suggesting an overall immune activation by thermal ablation[31,32]. Our results are consistent with the published paper in which photothermal therapy facilitated the accumulation and effector function of CAR T cells within solid tumors. More importantly, as a thermo ablative technology, MWA offers several advantages over surgical resection: lower morbidity, increased preservation of surrounding tissues, reduced cost and shorter hospitalization times[33], as well as intra-procedural monitoring by visualization, not to mention the ability to repeatedly treat patients who are not candidates for conventional therapies[27,30]. Altogether, MWA, as a commonly used method in clinical practice, combined with YW327.6S2-CAR T cell immunotherapy would have great translational value.

Our previous study showed that AXL upregulation correlated with acquired EGFR-TKI resistance[17] and YW327.6S2, an anti-AXL mAb, had also been indicated to enhance the antitumor efficacy of erlotinib[19]. We therefore investigated whether YW327.6S2 armored CAR T cells could robust the efficacy of erlotinib in an erlotinib-resistant (HCC827-ER3) tumor xenograft NSG mouse model. As expected, the results demonstrated that combination of YW327.6S2-CAR T cells indeed enhanced the therapeutic efficacy of erlotinib on HCC827-ER3 subcutaneous tumor. Interestingly, we found that YW327.6S2-CAR T cells downregulated the AXL expression, which might restore the erlotinib sensitivity in HCC827-ER3 tumor model (Fig. 7). Previous report using the first-in-human study of epidermal growth factor receptor variant III–redirected (EGFRvIII-redirected) CAR T cell therapy against glioblastoma showed that most of patients had specific loss or decrease of EGFRvIII-target antigen expression in tumors resected after CAR T cell infusion[34]. A preclinical study combining mesothelin-CAR T cells and cytokine-armed oncolytic adenoviruses indicated similar antigen intensity decrease in treating pancreatic cancer [35]. These findings support the idea that additional therapies enhancing antitumor efficacy, such as our approach to combine erlotinib with CAR T cells, may be valuable to prevent antigen escape. Recent phase I clinical trial revealed that bispecific anti-CD20, anti-CD19 CAR T cells may improve clinical responses by mitigating target antigen downregulation for relapsed B cell malignancies[36]. In this study, combining CAR T cells and erlotinib therapy showed the capability to lysing AXL-positive HCC827-ER3 cells, meanwhile, erlotinib

itself can target and suppress AXL-low or -negative tumor cells, which is a unique advantage of this combination strategy to overcome tumor heterogeneity. This type of cooperativity might be a promising treatment manner for AXL-CAR T therapy, especially for EGFR-TKI resistant tumor.

In summary, we characterized AXL as a target antigen of CAR T cells in human NSCLC and utilized the third-generation anti-AXL CAR T cells to target human NSCLC. Our data demonstrated that AXL-CAR T cells alone could exert potent antitumor activities and good safety profile against NSCLC. AXL-CAR T cells combined with MWA or erlotinib showed obvious synergistic effect for subsets of NSCLCs. These data demonstrated the potential translational value of employing AXL-CAR T cells alone or in combination to treat NSCLC patients, especially for EGFR-TKI resistant lung cancer in the clinic. Phase I clinical trial to further evaluate the safety of AXL-targeted CAR T cells is warranted.

Materials And Methods

Study design

The overall objective of this study was to demonstrate that AXL is a suitable target for CAR T cell therapy against NSCLC, alone or in combination strategy. We designed three types of AXL-targeted chimeric antigen receptors that, when transduced into human T cells, provided tumor antigen recognition and antigen-specific effector function. In vitro, we investigated (i) AXL expression in NSCLC cell lines, non-tumor tissues, matched tumor and paracarcinoma tissues via flow cytometry, western blot (WB), or immunohistochemistry (IHC), (ii) cytotoxicity and, (iii) cytokine secretion. All in vitro assays were performed with at least triplicate samples. We identified the best CAR constructs for in vivo studies based on their in vitro killing potency. We mainly analyzed the killing efficacy of YW327.6S2-CAR T cells, alone or in a combination manner. We developed subcutaneous, lung and abdominal metastatic tumor models via NSG immunodeficient mice with human NSCLC cells ($n \geq 5$), in order to mimic different clinical metastatic situation. Tumor challenged mice were randomized divided into treatment groups. Subcutaneous and lung metastatic tumor model were treated by CAR T cells via tail vein, while abdominal metastatic were administrated by intraperitoneal or intravenous injection, to optimize delivery methods. We also evaluated the efficacy, safety and synergistic mechanism of YW327.6S2-CAR T cells combined with thermal ablation (MWA) or erlotinib, in order to validate and facilitate the translation value of AXL-CAR T to the clinical application by combination modality. Tumor burden was monitored via calipers or living image. CAR T cell infiltration was detected via flow cytometry. Veterinary staff, independent of the researchers and studies, monitored mice daily and alerted researcher when a humane endpoint had been reached. All animal experiments were carried out according to the applicable guidelines and regulations approved by the Second Affiliated Hospital of Guangzhou Medical University Experimental Animal Care Commission.

1. **Cells lines**

A549, HCC827, and HEK-293T cell lines were obtained from the American Type Culture Collection. Erlotinib-resistant HCC827-ER3 cell line was established in Case Western Reserve University (Cleveland,

Ohio, USA) as previously described[17]. Cells were maintained in a humidified atmosphere containing 5% CO_2 at 37 °C. DMEM (Gibco) or RPMI-1640 (Gibco) with 10% FBS (Gibco), 100 IU/mL of penicillin (Gibco), and 100 IU/mL of streptomycin (Gibco), was used to culture all cancer cell lines. For in vitro cytotoxicity and in vivo living image experiment, A549, HCC827 and HCC827-ER3 cells were lentivirally transduced with pWPXLD-Luc(+)/eGFP virus expressing the GFP and luciferase (GL) genes. All cells were routinely tested for mycoplasma contamination.

2. **Affinity verification of Anti-AXL scFv**

The anti-AXL scFv was expressed and purified according to the instruction as previously described[37]. Briefly, the anti-AXL scFv was expressed by transient transfection of the plasmids with polyethyleneimine (MW25000, Polyscience) in Free-style 293-F cells (Invitrogen). The expressed scFv proteins were purified by protein A agarose beads (GE Healthcare). Affinity verification was achieved via ELISA.

3. **Vector design and lentivirus production**

To generate CARs targeting AXL, the genes of three anti-AXL scFv[18,19,23,24] and anti-CD19 (control scFv), followed by CD8 leader, CD8 hinge, CD28 transmembrane, and composite CD28-CD137-CD3ζ intracellular signaling domains, under the control of an EF-1α promoter, were codon optimized and synthesized by Genscript Co. Ltd. (Nanjing, China), then subcloned into the backbone lentiviral vector pWPXLd-2A-eGFP. The sequence of each cloned CAR was verified via sequencing.

Lentivirus particles were produced in HEK-293T cells after polyethyleneimine (Sigma-Aldrich)-mediated transfection with the constructed vector, together with two auxiliary packaging plasmids, psPAX2 and pMD.2G. Supernatants were harvested at 48 and 72 h post-transfection and filtered through a 0.45-μm filter (Millipore) to remove cell debris.

4. **Isolation, transduction, and expansion of primary human T lymphocytes**

Peripheral blood mononuclear cells (PBMCs) were isolated from the buffy coats of healthy donors using Lymphoprep (Stemcell). T cells were positively selected from PBMCs using a MACS Pan T Cell Isolation Kit (Miltenyi Biotec) and activated using microbeads coated with anti-human CD3/CD28, (Miltenyi Biotec) at a 1:1 bead:cell ratio for 24-72 h in T cell medium (Miltenyi Biotec). Transduction were performed as previously described[38]. Transduction efficiency was determined after 72 h by the percentage of GFP+ cells via flow cytometry. T cell phenotype was examined before and after transduction. Informed consents from healthy PBMC donors were obtained, and all procedures were approved by the Research Ethics Board of The Second Affiliated Hospital of Guangzhou Medical University.

5. **Quantitative real-time polymerase chain reaction (qPCR)**

The expression of different CAR mRNAs was detected by quantitative real-time polymerase chain reaction (qPCR), as previously described. The glyceraldehyde-3-phosphate dehydrogenase (GAPDH) gene was

used as an endogenous control. The primers for different CARs were:

GAPDH - sense: 5’- GCACCGTCAAGGCTGAGAAC-3’

GAPDH - antisense: 5’- TGGTGAAGACGCCAGTGGA -3’

scFv of 3E3E8 - sense: 5’- GCACAGCAACGGCAACACCTA-3’

scFv of 3E3E8 - antisense: 5’- CCGCTAAACCTATCGGGCACT -3’

scFv of YW327.6S2 - sense: 5’- GCAGCATCTGGCTTTTCTC -3’

scFv of YW327.6S2 - antisense: 5’- TTCACGGAGTCGGCATAGT -3’

scFv of 20G7D9 - sense: 5’- TACAATGAGAAGTTCAACGACCG -3’

scFv of 20G7D9 - antisense: 5’- GTCCCCAGTATGCGAACCAG -3’

scFv of CD19 - sense: 5’- ACTACATCCTCCCTGTCTGCC - 3’

scFv of CD19 - antisense: 5’- CCACTGCCACTGAACCTTGA - 3’

6. **Flow cytometry**

All samples were analyzed using a NovoCyteTM (ACEA Biosciences), and data were analyzed using FlowJo software (FlowJo). The antibodies used included anti-AXL-PE (clone DS7HAXL) (Invitrogen), anti-human CD3-FITC (clone UCHT1), anti-human CD4-APC (clone RPA-T4), anti-human CD8a-PE (clone HIT8a). All FACS-related staining procedures were performed on ice for 30 min, and cells were then washed with PBS containing 1% FBS before cytometry analysis. PB and tumor samples from mouse xenografts were treated with red blood cell lysis buffer (Thermo Fisher Scientific), and the cells were stained with the corresponding antibodies.

7. **In vitro cytotoxicity and cytokine release assay**

A549 GL, HCC827 GL, and HCC827-ER3 GL target cells were incubated with Mock, CD19- or three AXL-CAR T cells at the indicated effector to target (E:T) ratios of 8:1, 4:1, 2:1, and 1:1 in triplicate wells of U-bottomed 96-well plates at 37°C. Target cell viability was monitored 24 h later by adding 100 μL/well D-Luciferin (Cayman Chemical) resolved at 150 μg/mL. Then, the viability percentage (%) was calculated as experimental signal/maximal signal × 100, and the specific cell lysis was calculated using 100%-viability percentage.

Target cells (1×10^4) were incubated with effector cells (1×10^4) in U-bottomed 96-well plates for 24 h. The culture supernatants were then collected and analyzed for the secretion of IL-2, TNF-α, IFN-γ, GM-CSF, Granzyme B, and Perforin using enzyme-linked immunosorbent assay (ELISA) kits (R&D Systems) according to the manufacturer’s protocol.

8. **IHC and Western blot analysis**

IHC and Western Blot procedures were performed following the standard protocols. Sample collecting was approved by the Research Ethics Board of The Second Affiliated Hospital of Guangzhou Medical University.

Different levels of AXL expression in 90 paraffin-embedded NSCLC tissue (including 40 erlotinib resistant cases) and 22 kinds of non-tumor paraffin-embedded samples (detailed in Supplementary Table 1), were evaluated by one experienced pathologist using a 4-point scale. Score 0 means no AXL expression; scores of 1+, 2++, and 3+++ mean weak to strong expression of AXL. The percentages of AXL-positive staining with different scores were also recorded.

For Western Blot (WB), membranes were probed with anti-human AXL (Cell Signaling Technology), anti-human CD3 (Abcam) primary antibodies.

9. **In Vivo Antitumor Studies**

Six- to eight-week-old female NSG (NOD-Prkdc^{scid}IL2rg^{tm1}/Bcgen, Biocytogen, Beijing, China) mice were housed and treated under specific pathogen-free conditions and were provided autoclaved food and water at the Experimental Animal Center of The Second Affiliated Hospital of Guangzhou Medical University (Guangzhou, China). All animal experiments were carried out according to the applicable guidelines and regulations approved by The Second Affiliated Hospital of Guangzhou Medical University Experimental Animal Care Commission. For the following in vivo studies, tumor volume was measured every three days with a caliper and calculated with the following equation: tumor volume= (length×width^2)/2, or monitored via bioluminescence imaging (BLI) for tumor progression. To improve the CAR T cell percentage of primary T cells, transduction by lentivirus was performed twice or thrice before in vivo assay.

For the cell line-based/derived NSCLC subcutaneous xenograft models, 2×10^6 A549 or HCC827-ER3 cells in 100 μL PBS were subcutaneously injected into the right flanks of NSG mice on day 0. When tumor nodes reached about 50 mm^3, the mice were divided into three groups: Mock, CD19-CAR T and AXL-CAR T (n=6), and received PBS or 1×10^7 CAR T (CD19- or YW327.6S2-CAR T) cells intravenously. On day 39 (A549) and 45 (HCC827-ER3) after tumor inoculation, all mice were sacrificed. Tumor weight was measured.

In order to construct pulmonary and intraperitoneal metastasis models, 1×10^6 A549 GL cells in 100 μL PBS were injected into NSG mice intravenously (i.v.) or intraperitoneally (i.p.), respectively, on day 0. Two weeks after tumor cells injection, the mice were subjected to BLI. For lung metastasis, mice were randomly divided into (n=5): Mock, CD19-CAR T and AXL-CAR T. Mice were administrated with PBS (Mock), or 1×10^7 effector cells (CD19- or YW327.6S2-CAR T) suspended in 100 μL PBS intravenously injected on day 14. For intraperitoneal metastasis models, mice were randomly assigned into (n=5): Mock, YW327.6S2-CAR T (i.v.), and YW327.6S2-CAR T (i.p.). Mice were administrated with PBS (Mock), or

1×10^7 YW327.6S2-CAR T cells (i.v. or i.p.) suspended in 100 μL PBS (i.p.) on day 14. Mice were monitored with BLI frequently for disease progression. T cell percentages in peripheral blood was detected by flow cytometry.

To assess synergistic antitumor efficacy of combination therapy, subcutaneous tumor model by inoculating HCC827-ER3 or HCC827-ER3 GL cells was established (day 0). For YW327.6S2-CAR T cells combined with MWA modality (Vision-China Medical Devices R&D center), experiment was initiated when mean tumor volume reached about 200 mm^3, mice were then randomly allocated to four groups (n=5): Mock (PBS), MWA (10w, 45s, on day 30), YW327.6S2-CAR T (1×10^7 YW327.6S2-CAR T cells, on day 30, i.t.), and combination groups (ablation, on day 30, combined with 5×10^6 YW327.6S2-CAR T cells, on day 33, i.t.). To reach partial ablation, a time-power gradient experiment was performed, in order to faithfully mimic the tumor residue or marginal recurrence after ablation. Tumor volume and weight was measured. Blood was collected for biochemistry analysis. T cell infiltration in peripheral blood and tumor was tested by flow cytometry. Ki-67 expression in tumor tissue was detected via IHC. At the same time, all important mouse organs, including heart, liver, spleen, lung, kidney, cerebrum, stomach, small intestine and colon, were harvested, fixed with 4% paraformaldehyde and stained with hematoxylin-eosin (H&E) or corresponding antibodies (IHC). For YW327.6S2-CAR T cells combined with erlotinib tactics, experiment was carried out when mean tumor volume reached about 100 mm^3, mice were randomly divided into four groups (n=5): Mock, erlotinib, YW327.6S2-CAR T (1×10^7 YW327.6S2-CAR T cells, i.v.), and combination groups (erlotinib combined with 5×10^6 YW327.6S2-CAR T cells, i.v.). Erlotinib was administrated by gavage (100mg/kg/day) on day 21 to 42, YW327.6S2-CAR T cells were injected intravenously on day 21. AXL expression were detected in dissected tumor after euthanasia.

10. **Bioluminescence imaging**

Isoflurane-anesthetized animals were imaged using a cooled CCD camera system (IVIS 100 Series Imaging System, Xenogen), followed by the intraperitoneal injection of 75 mg/kg D-luciferin (Cayman Chemical). Quantification of total and average emissions were quantified using Living Image software (Xenogen).

11. **Statistics**

Data were presented as mean ± SD or SEM. Differences between groups were analyzed by one-way ANOVA with Bonferroni post-tests. Gray-scale analysis of WB was achieved by ImageJ. The Kruskal-Wallis test was utilized to compare the non-normally distributed endpoints. For survival data, Kaplan-Meier curves were plotted and compared using a log-rank test. GraphPad Prism 7.0 was used for the statistical calculations. *$p < 0.05$, **$p < 0.01$, and ***$p < 0.001$ were considered statistically significant.

References

1. Herbst, R.S. et al. The biology and management of non-small cell lung cancer. *Nature* **553**, 446-454 (2018).
2. Siegel, R.L. et al. Cancer Statistics, 2021. *CA: a cancer journal for clinicians* **71**, 7-33 (2021).
3. Mayekar, M.K. & Bivona, T.G. Current Landscape of Targeted Therapy in Lung Cancer. *Clinical pharmacology and therapeutics* **102**, 757-764 (2017).
4. Jamal-Hanjani, M. et al. Tracking the Evolution of Non-Small-Cell Lung Cancer. *The New England journal of medicine* **376**, 2109-2121 (2017).
5. Grupp, S.A. et al. Chimeric antigen receptor-modified T cells for acute lymphoid leukemia. *The New England journal of medicine* **368**, 1509-1518 (2013).
6. Porter, D.L. et al. Chimeric antigen receptor-modified T cells in chronic lymphoid leukemia. *The New England journal of medicine* **365**, 725-733 (2011).
7. Wang, Z. et al. Current status and perspectives of chimeric antigen receptor modified T cells for cancer treatment. *Protein & cell* **8**, 896-925 (2017).
8. Zhang, Q. et al. CAR-T cell therapy in gastrointestinal tumors and hepatic carcinoma: From bench to bedside. *Oncoimmunology* **5**, e1251539 (2016).
9. Li, J. et al. Chimeric antigen receptor T cell (CAR-T) immunotherapy for solid tumors: lessons learned and strategies for moving forward. *Journal of hematology & oncology* **11**, 22 (2018).
10. Priceman, S.J. et al. Regional Delivery of Chimeric Antigen Receptor-Engineered T Cells Effectively Targets HER2 Breast Cancer Metastasis to the Brain. *Clinical cancer research : an official journal of the American Association for Cancer Research* **24**, 95-105 (2018).
11. Tchou, J. et al. Safety and Efficacy of Intratumoral Injections of Chimeric Antigen Receptor (CAR) T Cells in Metastatic Breast Cancer. *Cancer immunology research* **5**, 1152-1161 (2017).
12. Adusumilli, P.S. et al. Regional delivery of mesothelin-targeted CAR T cell therapy generates potent and long-lasting CD4-dependent tumor immunity. *Science translational medicine* **6**, 261ra151 (2014).
13. Brown, C.E. et al. Regression of Glioblastoma after Chimeric Antigen Receptor T-Cell Therapy. *The New England journal of medicine* **375**, 2561-2569 (2016).
14. Chen, Q. et al. Photothermal Therapy Promotes Tumor Infiltration and Antitumor Activity of CAR T Cells. *Advanced materials (Deerfield Beach, Fla.)* **31**, e1900192 (2019).
15. Yu, H. et al. Axl receptor tyrosine kinase is a potential therapeutic target in renal cell carcinoma. *British journal of cancer* **113**, 616-625 (2015).
16. Li, D. et al. Axl-targeted cancer imaging with humanized antibody h173. *Molecular imaging and biology* **16**, 511-518 (2014).
17. Zhang, Z. et al. Activation of the AXL kinase causes resistance to EGFR-targeted therapy in lung cancer. *Nature genetics* **44**, 852-860 (2012).
18. Leconet, W. et al. Preclinical validation of AXL receptor as a target for antibody-based pancreatic cancer immunotherapy. *Oncogene* **33**, 5405-5414 (2014).

19. Ye, X. et al. An anti-Axl monoclonal antibody attenuates xenograft tumor growth and enhances the effect of multiple anticancer therapies. *Oncogene* **29**, 5254-5264 (2010).
20. Cho, J.H. et al. Universal Chimeric Antigen Receptors for Multiplexed and Logical Control of T Cell Responses. *Cell* **173**, 1426-1438.e1411 (2018).
21. Wei, J. et al. A novel AXL chimeric antigen receptor endows T cells with anti-tumor effects against triple negative breast cancers. *Cellular immunology* **331**, 49-58 (2018).
22. Cho, J.H. et al. Engineering Axl specific CAR and SynNotch receptor for cancer therapy. *Scientific reports* **8**, 3846 (2018).
23. Pei, L. et al. Anti-Axl antibodies and methods of use. United States patent US 8853369 B2.
24. Bruno, R. et al. Anti-Axl antibodies and uses thereof. United States patent US 20140302041 A1.
25. Springuel, L. et al. Chimeric Antigen Receptor-T Cells for Targeting Solid Tumors: Current Challenges and Existing Strategies. *BioDrugs : clinical immunotherapeutics, biopharmaceuticals and gene therapy* **33**, 515-537 (2019).
26. Linger, R.M. et al. Mer or Axl receptor tyrosine kinase inhibition promotes apoptosis, blocks growth and enhances chemosensitivity of human non-small cell lung cancer. *Oncogene* **32**, 3420-3431 (2013).
27. Dupuy, D.E. Image-guided thermal ablation of lung malignancies. *Radiology* **260**, 633-655 (2011).
28. Ahmed, M. et al. Principles of and advances in percutaneous ablation. *Radiology* **258**, 351-369 (2011).
29. Silvestrini, M.T. et al. Priming is key to effective incorporation of image-guided thermal ablation into immunotherapy protocols. *JCI insight* **2**, e90521 (2017).
30. Chu, K.F. & Dupuy, D.E. Thermal ablation of tumours: biological mechanisms and advances in therapy. *Nature reviews. Cancer* **14**, 199-208 (2014).
31. Dromi, S.A. et al. Radiofrequency ablation induces antigen-presenting cell infiltration and amplification of weak tumor-induced immunity. *Radiology* **251**, 58-66 (2009).
32. Rughetti, A. et al. Modulation of blood circulating immune cells by radiofrequency tumor ablation. *Journal of experimental & clinical cancer research : CR* **22**, 247-250 (2003).
33. Pereira, P.L. Actual role of radiofrequency ablation of liver metastases. *European radiology* **17**, 2062-2070 (2007).
34. O'Rourke, D.M. et al. A single dose of peripherally infused EGFRvIII-directed CAR T cells mediates antigen loss and induces adaptive resistance in patients with recurrent glioblastoma. *Science Translational Medicine* **9**, eaaa0984 (2017).
35. Watanabe, K. et al. Pancreatic cancer therapy with combined mesothelin-redirected chimeric antigen receptor T cells and cytokine-armed oncolytic adenoviruses. *JCI insight* **3**(2018).
36. Shah, N.N. et al. Bispecific anti-CD20, anti-CD19 CAR T cells for relapsed B cell malignancies: a phase 1 dose escalation and expansion trial. *Nature Medicine* **26**, 1569-1575 (2020).

37. Li, D. et al. N-terminal α-amino group modification of antibodies using a site-selective click chemistry method. *mAbs* **10**, 712-719 (2018).
38. Lv, J. et al. Mesothelin is a target of chimeric antigen receptor T cells for treating gastric cancer. *Journal of hematology & oncology* **12**, 18 (2019).

Declarations

Acknowledgements

We thank Q. Zhao (University of Macau) for the expression and purification of AXL scFv proteins. We thank P. Li (University of Chinese Academy of science) for kindly endow the backbone lentiviral vector pWPXLd-2A-eGFP. This research was supported by the National Natural Science Foundation of China (No. 81672276) and Guangzhou Municipal Science and Technology Project (No. 201803010038).

Author contributions

B.C., M.L., Y.Z., H.L., D.C., L.Y. and Z.Z. conceived and designed the project and contributed to the interpretation of data. Q.Z., L.W., B.L., J.Z., J.L., X.C., Y.F., C.Z., X.Y., Y.T., Y.H., J.H., H.H., X.Y. and G.Z. contributed to the acquisition and analysis of data. B.C., M.L. and Y.Z. drafted the manuscript. Z.Z., L.Y., D.C., H.L, M.Z., L.X., Q.W. and A.C. revised and supervised the manuscript.

Competing interests

No other authors declare any competing financial interests. No authors declare any nonfinancial interests.

Figures

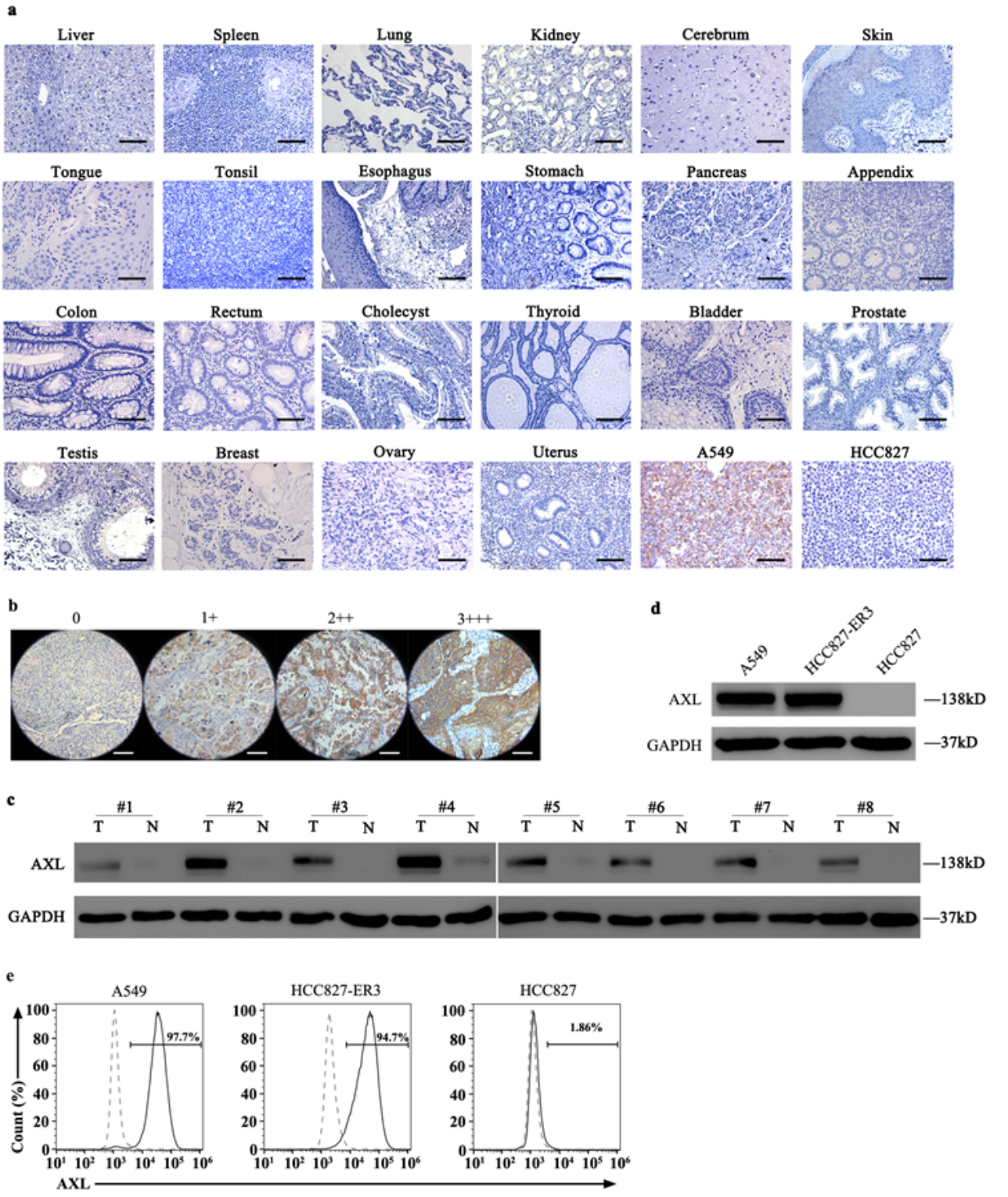

Figure 1

Analysis of AXL expression in human non-tumor and NSCLC tissues and lung cancer cell lines. a, Twenty two different human non-tumor tissue samples were immunostained with an anti-AXL antibody to determine the expression level of AXL protein. Representative staining images (magnification × 400) are shown. Scale bars represent 100 μm. Paraffin-embedded A549 and HCC827 cells served as positive and negative AXL staining, respectively. b, Levels of AXL expression were evaluated using a 4-point scale in

90 NSCLC samples (including 40 EGFR-TKI resistant tissues) by immunohistochemistry staining. Representative images (magnification × 400) are shown. Scale bars represent 100 μm. c, Detection of AXL expression in 8 pairs of NSCLC with EGFR-TKI resistant fresh tissues (T) and adjacent normal lung tissues (N) by Western Blotting. d and e, Detection of AXL expression in human NSCLC cell lines, A549, HCC827-ER3, and HCC827 by Western Blotting (d) and flow cytometry (e).

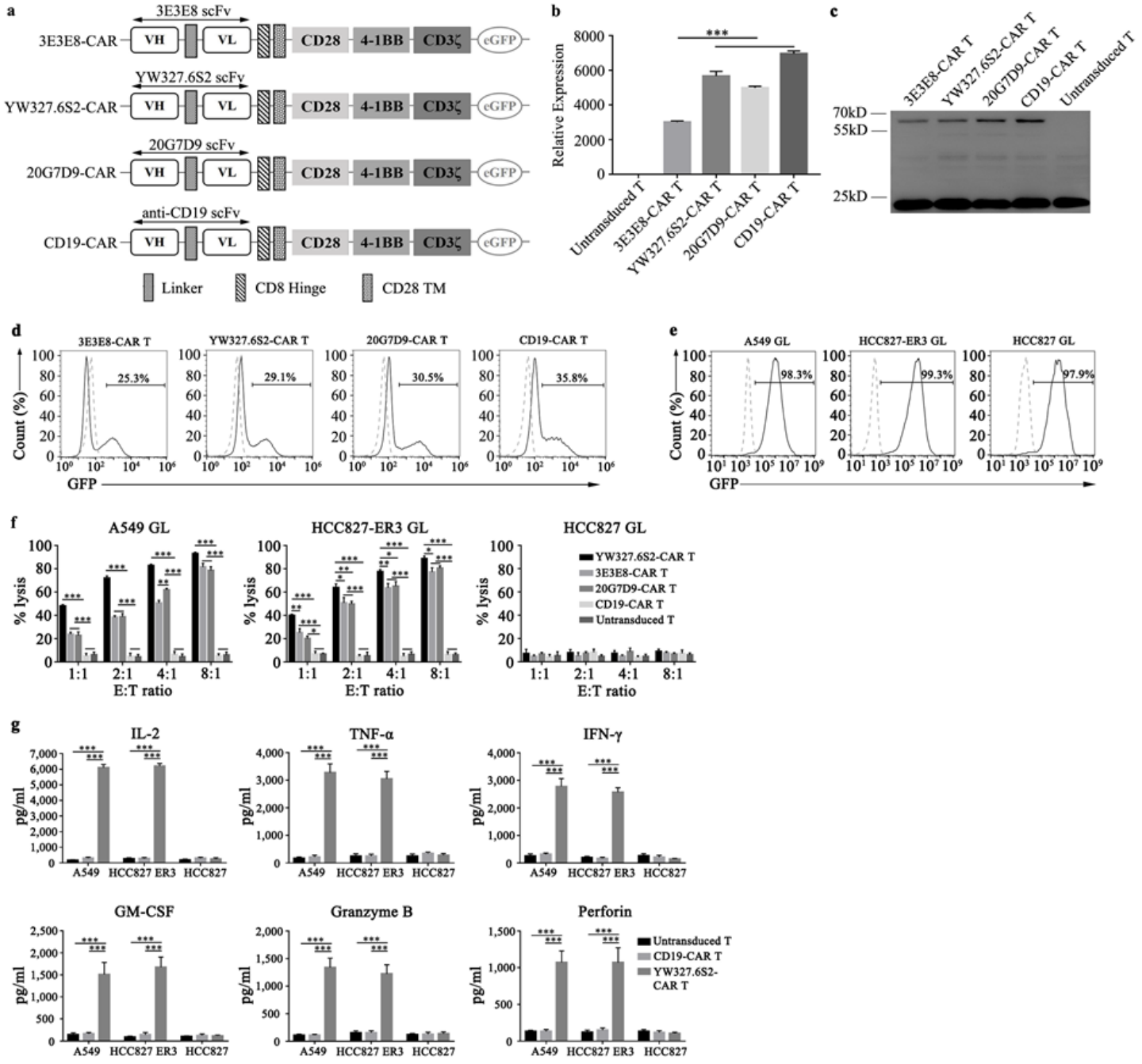

Figure 2

Generation of CAR T cells and their anti-cancer cytotoxicity assay in vitro. a, Schematic diagram of the AXL- and CD19-CAR transgene domains. b, Relative expressions of different CAR mRNAs normalized to GAPDH in CAR T cells were detected by qPCR. Data are expressed as means ± SEM of triplicate samples.

c, Western blotting analysis of CAR expression in transduced AXL- and CD19-CAR T cells. A CD3 ζ-specific antibody was used to detect endogenous and chimeric CD3 ζ. d, Percentage of AXL- and CD19-CAR transduced CAR T cells detected by flow cytometry. GFP served as a marker of CAR expression. Dash line indicated isotype control. e, GFP and Luciferase (GL) expression was detected in A549 GL, HCC827-ER3 GL, and HCC827 GL cells by flow cytometry. GFP served as a marker of luciferase expression. f, Antitumor cytotoxicity assay of AXL-CAR T cells. The effector T cells were co-cultured for 24 hrs with target cells (1×104) at effector (E): target (T) ratios of 1:1, 2:1, 4:1, and 8:1 in a total volume of 100 μL. g, Detection of IL-2, TNF-α, IFN-γ, GM-CSF, Granzyme B, and Perforin secretion by effector cells after coculture with target cells for 24 hrs at an E:T ratio of 1:1. Data are expressed as mean±SEM of three separate experiments. *p < 0.05, **p < 0.01, and ***p < 0.001.

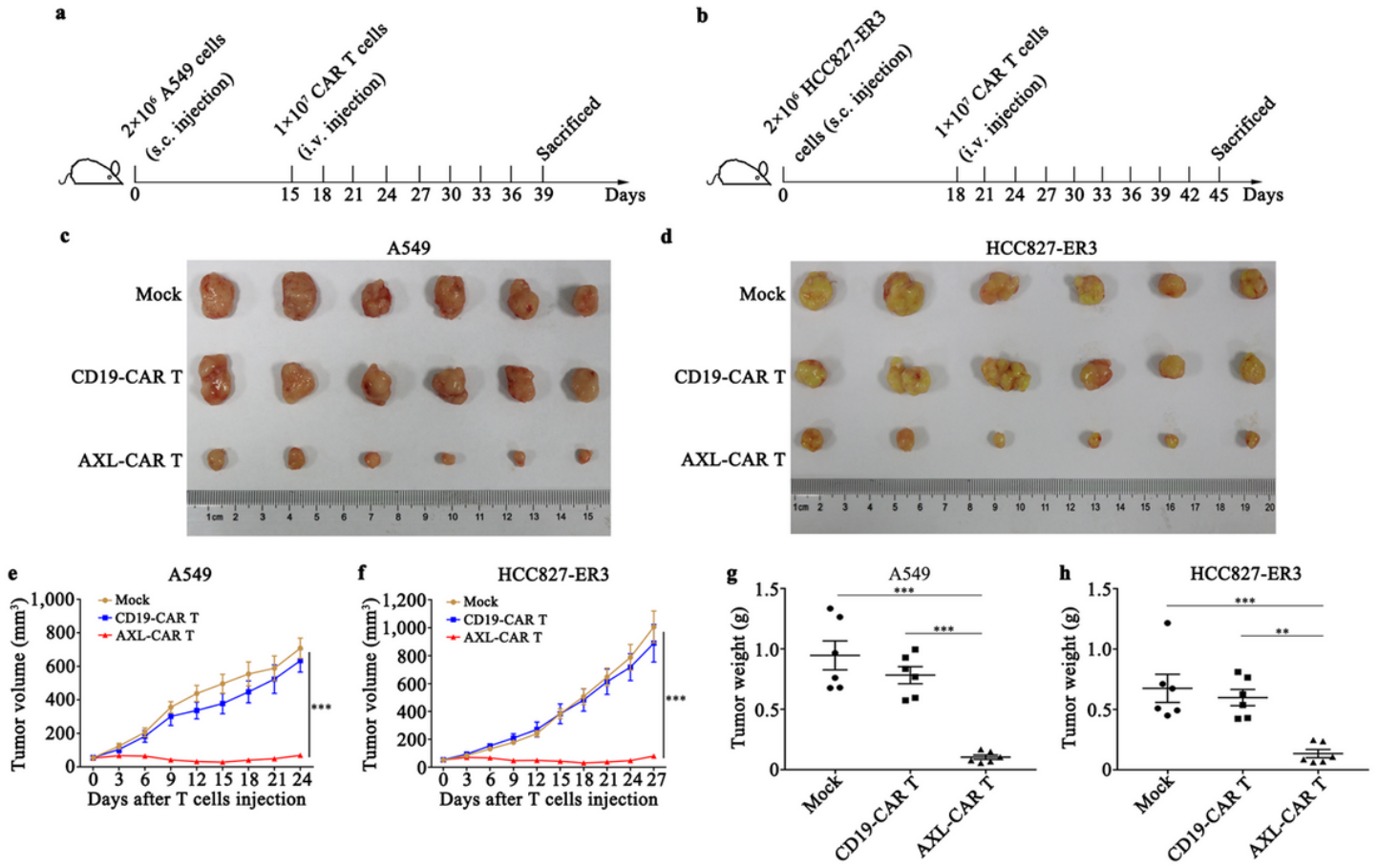

Figure 3

AXL-CAR T cells showed antitumor activity in subcutaneous mouse models. a and b, Schemes of experiments for A549 and HCC827-ER3 bearing mice. NSG mice received a subcutaneous injection of 2×106 A549 or HCC827-ER3 cells. When tumor volume reached 50 mm3, 1×107 YW327.6S2-CAR T cells or equivalent numbers of CD19-CAR T cells were injected through the tail vein and tumor volume was measured every three days. c and d, Tumors from different groups at the end point. e and f, Tumor volume in A549 and HCC827-ER3 subcutaneously injected mice. Tumor volume=(length×width2)/2. g

and h, Tumor weight in A549 and HCC827-ER3 subcutaneous model at the end point. Mock=PBS. Error bars denote the SD. *p < 0.05, **p < 0.01, ***p < 0.001.

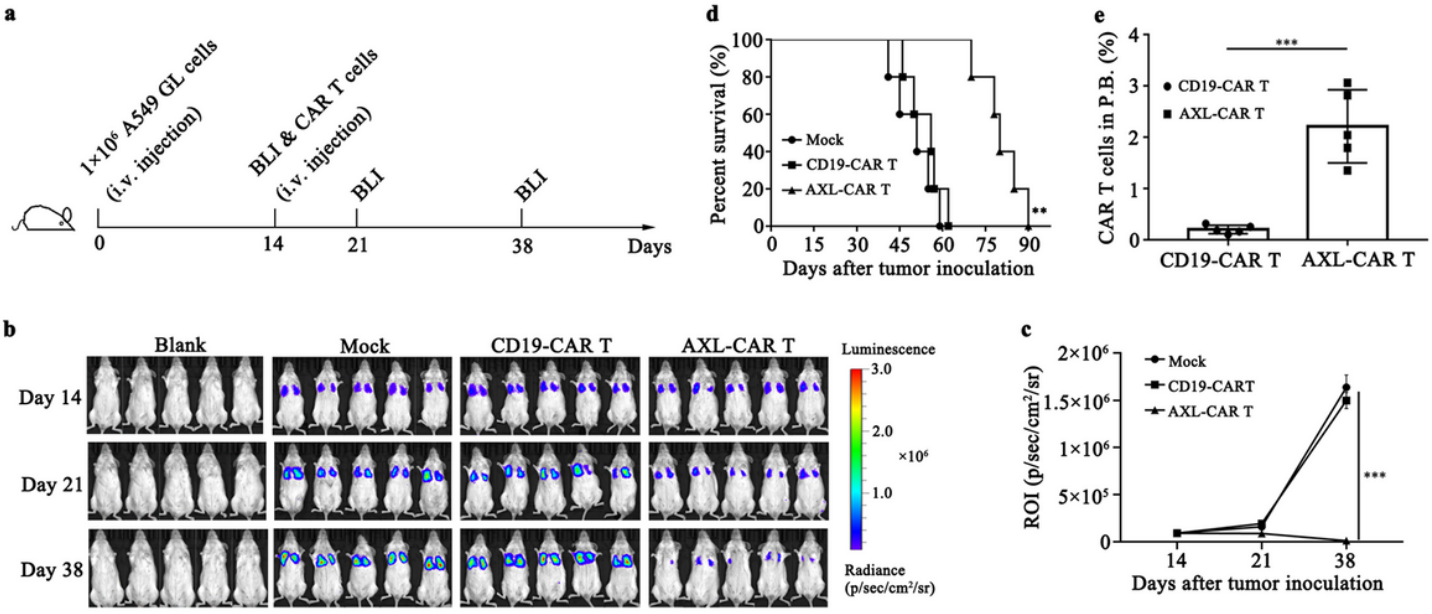

Figure 4

YW327.6S2-CAR T cells showed strong antitumor activity in a pulmonary metastatic NSCLC model. a, Schematic representation of the experiment. b, Bioluminescence imaging (BLI) of A549 GL intravenously injected mice treated with CD19- or YW327.6S2-CAR T cells. Briefly, NSG mice received an i.v. injection of 1×106 A549 GL cells. After 14 days, 1×107 YW327.6S2-CAR T cells or equivalent number of CD19-CAR T cells were injected through the tail vein, and BLI was conducted on day 14, 21, and 38. c, Statistical analysis of the ROI at each time point. Error bars denote the SD, and the results were compared with two-way ANOVA test. *P< 0.05; **P< 0.01; ***P<0.001. d, Survival curve of A549 GL bearing mice. The results were performed with Log-rank (Mantel-Cox) test. e, Percentage of T cells in the peripheral blood (P.B.) of A549 GL intravenously injected mice. Error bars denote the SD, and the results were compared with a Wilcoxon rank sum test. *P<0.05; **P<0.01; ***P<0.001.

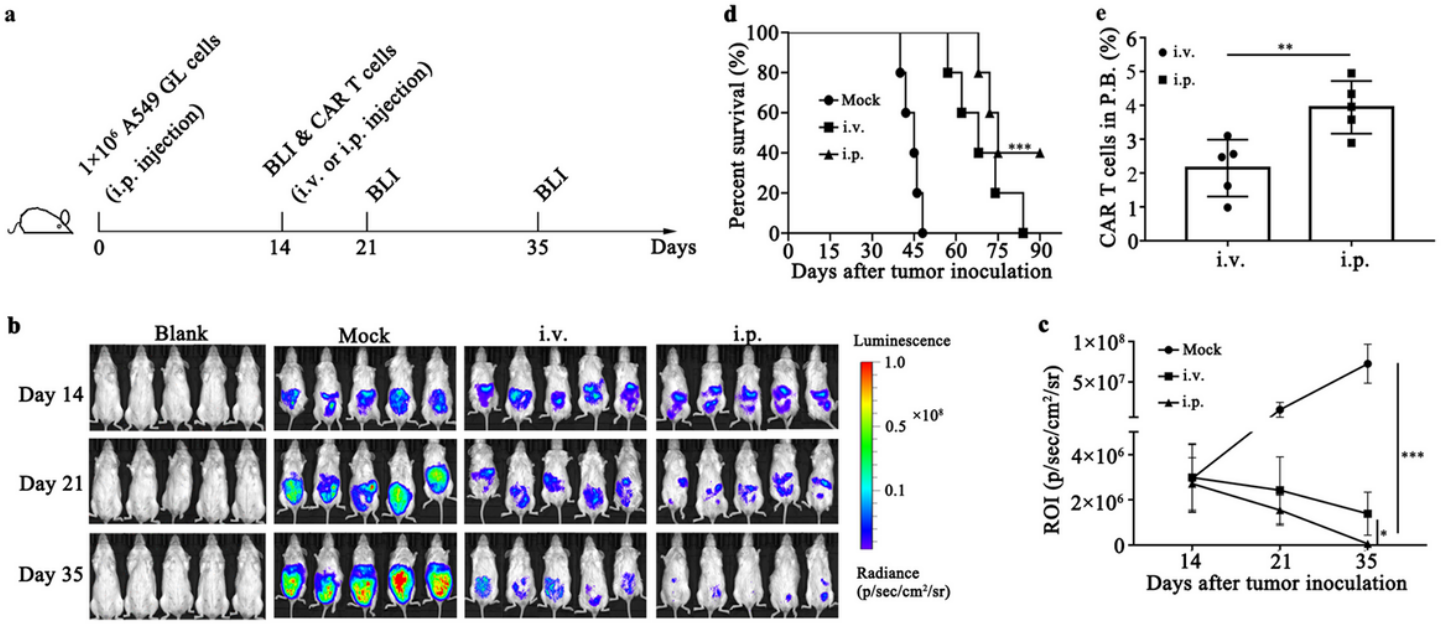

Figure 5

Regional delivery of CAR T cells was more effective in tumor killing than the systemic route. a, Schematic representation of the experiment. b, BLI of A549-GL intraperitoneally injected mice treated with YW327.6S2-CAR T cells (i.v. or i.p.). On day 0, NSG mice received an i.p. injection of 1 × 106 A549 GL cells. After 14 days, 1×107 YW327.6S2-CAR T cells were injected intravenously or intraperitoneally. On day 14, 21, and 35, BLI was conducted. c, Statistical analysis of the ROI of each BLI at each time point. Error bars denote the SD, and the results were compared with two-way ANOVA test. d, Survival curve of A549 GL intraperitoneally injected mice. The results were performed with Log-rank (Mantel-Cox) test. e, Percentage of T cells in the P.B. of A549 GL intraperitoneally injected mice. Error bars denote the SD, and the results were compared with a Wilcoxon rank sum test. *P<0.05, **P<0.01, ***P<0.001.

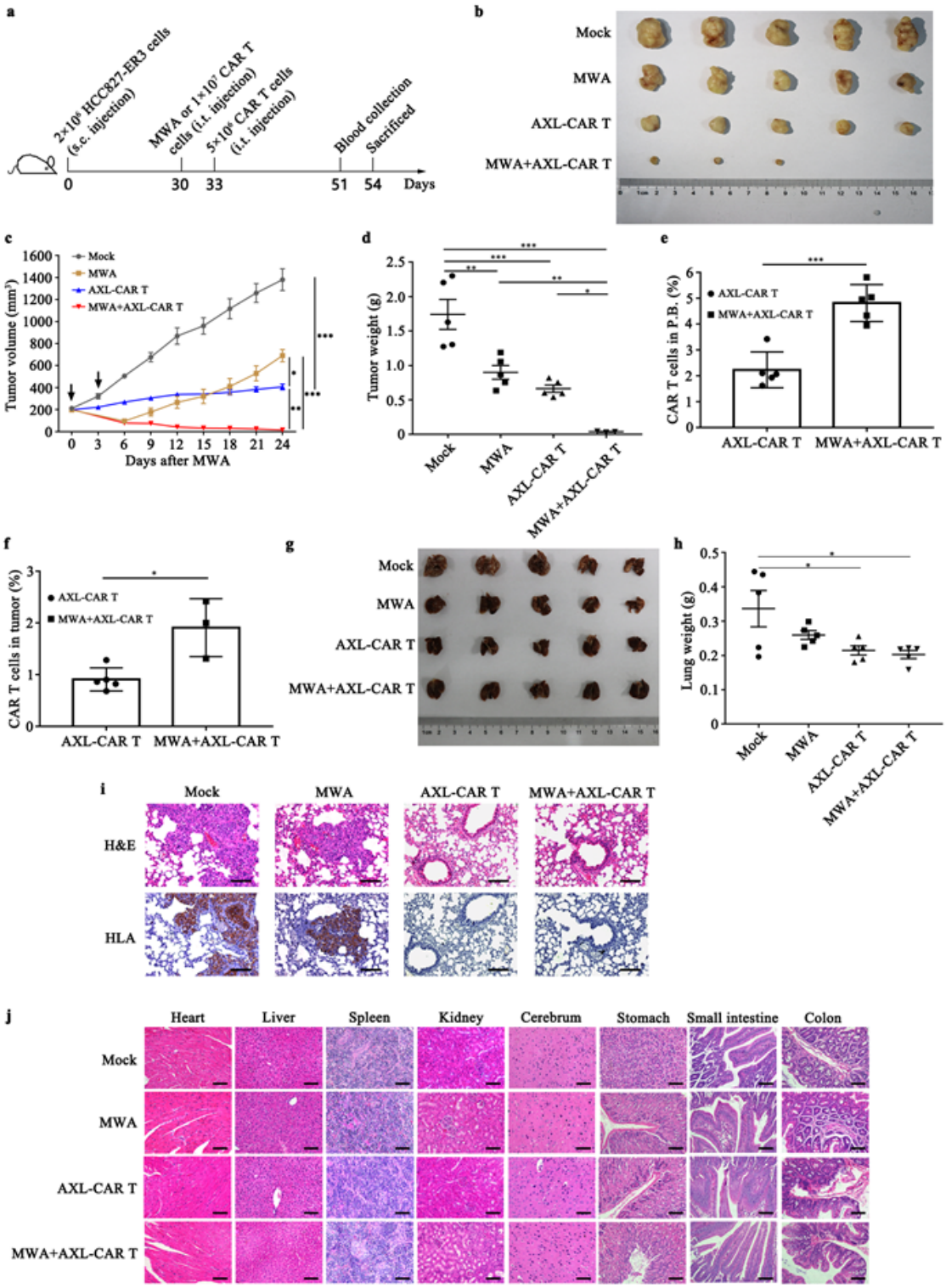

Figure 6

Microwave ablation promoted antitumor activity of CAR T cells against lung cancer and their infiltration in P.B. or tumor. a, Schematic representation of the experiment for MWA combined with YW327.6S2-CAR T cells. b, Tumors from different groups. c, Tumor volume of HCC827-ER3 subcutaneously injected mice. Tumor volume=(length×width2)/2. d, Mean tumor weight in each group at the end point. Error bars denote the SD. e and f, Percentage of T cells in the P.B. and tumor of HCC827-ER3 bearing mice. Error bars

denote the SD, and the results were analyzed by a Wilcoxon rank sum test. g, Combined MWA with YW327.6S2-CAR T cells prevented tumor metastasis. Representative lungs from mock, YW327.6S2-CAR T, MWA, and combination group are shown. The lungs with multiple metastases shown here were from mice treated with mock or MWA that were euthanized at day 54 due to weight loss. The lungs without metastasis were representative from mice treated with combination group and YW327.6S2-CAR T cells. h, The weight of lungs from each group. Error bars denote the SD. i, Detection of HLA expression in harvested lung tissues from each group. HLA was positively stained in lung tissues from mock and MWA group. j, Histopathological analysis of murine organ tissues by hematoxylin and eosin (H&E) staining. Different tissues were harvested, formalin-fixed, paraffin-embedded, and stained with H&E. Representative staining image fields (magnification × 400) are shown. Each scale bar represents 100μm. *p < 0.05, **p < 0.01, ***p < 0.001.

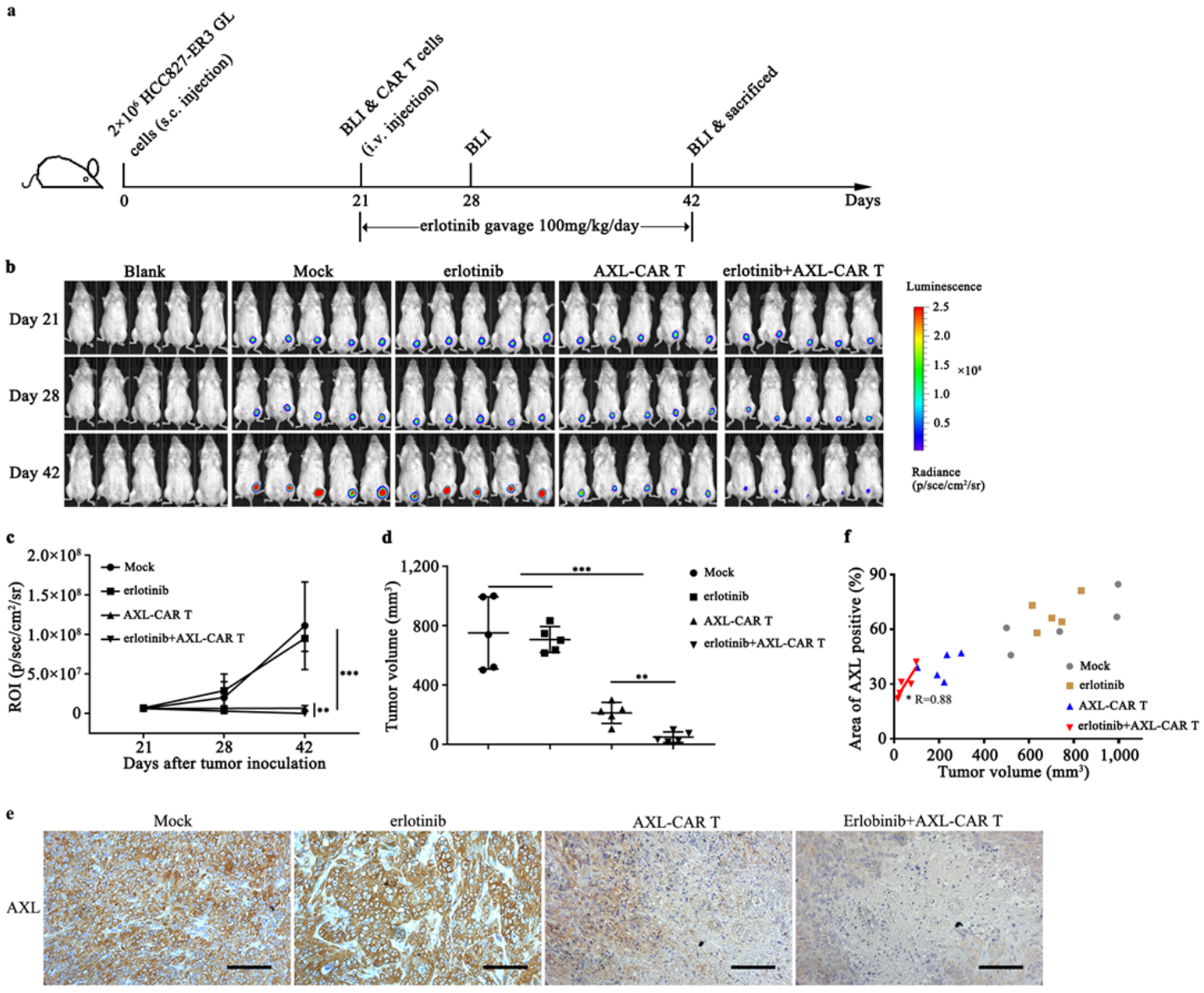

Figure 7

Therapeutic efficacy of YW327.6S2-CAR T cells combined with erlotinib for human NSCLC established with HCC827-ER3 GL cells. a, Schematic diagram showing the treatment program of the mice. b, BLI from different groups, using the treatment schedule shown in Figure 7a. c, Luminescence from tumor areas was quantified for the ROI of BLI at each time point. Error bars denote the SD, and the results were analyzed by two-way ANOVA test. *p < 0.05, **p < 0.01, ***p < 0.001. d, Tumor volume at the end of the treatment. Data were presented as the mean tumor volume ± SD. Statistical significance was calculated by one-way analysis of variance (ANOVA) with Bonferroni post test. e, Analysis of AXL expression in tumors by IHC at day 42. AXL-positive area and staining intensity were analyzed with Aperio ImageScope software. f, Correlation between AXL expression and tumor sizes. Areas of AXL positivity (%) were plotted against tumor size at day 42. Linear regression lines are shown. *P < 0.05, **P < 0.01.

Supplementary Files

This is a list of supplementary files associated with this preprint. Click to download.

- Ethicalapprovaldocuments.pdf
- SupplementaryMaterials.doc